ADVANCED MATERIALS
www.advmat.de

Morphogenic Growth 3D Printing

*Yun Seong Kim, Minjiang Zhu, Mohammad Tanver Hossain, Derrick Sanders, Rohan Shah, Yuan Gao, Jeffrey S. Moore, Nancy R. Sottos, Randy H. Ewoldt, Philippe H. Geubelle, and Sameh H. Tawfick**

Inspired by nature's morphogenesis, a new 3D printing process –growth printing (GP)– takes advantage of a self-propagating curing front to produce 3D polymeric parts following a growth-like development plan. The propagation of the curing front is driven by the exothermic polymerization of dicyclopentadiene (DCPD), which transforms the liquid resin into a stiff polymer as it propagates at 1 mm s^{-1}. GP is triggered when a heated initiator contacts the uncured liquid resin in an open container. The initiator nucleates the frontal polymerization reaction and the isotropic radial propagation of the growth front. Simultaneously, the initiator is moved up across the free surface of the resin, pulling the cured object out of the uncured resin. The motion trajectory of the initiator with respect to the free resin surface controls the growth morphology of the 3D part. An inverse design algorithm is developed to produce 3D parts by modeling the reaction-diffusion-driven solidification process. This process has substantial energy savings and high printing speeds.

Y. S. Kim, M. Zhu, M. T. Hossain, D. Sanders, R. Shah, Y. Gao, J. S. Moore, N. R. Sottos, R. H. Ewoldt, P. H. Geubelle, S. H. Tawfick
Beckman Institute for Advanced Science and Technology
University of Illinois at Urbana-Champaign
Urbana, IL 61801, USA
E-mail: tawfick@illinois.edu

Y. S. Kim, M. T. Hossain, D. Sanders, R. Shah, R. H. Ewoldt, S. H. Tawfick
Department of Mechanical Science and Engineering, Grainger College of Engineering
University of Illinois at Urbana-Champaign
Urbana, IL 61801, USA

M. Zhu, P. H. Geubelle
Department of Aerospace Engineering, Grainger College of Engineering
University of Illinois at Urbana-Champaign
Urbana, IL 61801, USA

Y. Gao
Huazhong University of Science and Technology
Wuhan, Hubei 430074, China

J. S. Moore, N. R. Sottos
Department of Material Science and Engineering, Grainger College of Engineering
University of Illinois at Urbana-Champaign
Urbana, IL 61801, USA

The ORCID identification number(s) for the author(s) of this article can be found under https://doi.org/10.1002/adma.202406265

DOI: 10.1002/adma.202406265

1. Introduction

The most widely used manufacturing process for polymeric parts is injection molding. Molding is cost-effective for mass production but cannot meet the demand for customized parts due to the high cost of machining and maintaining the metal molds and the molding equipment. Moreover, molds and curing ovens must be larger than the size of the parts produced, which becomes impractical for large parts such as the hulls of boats or the blades of wind turbines.[1]

The introduction of additive manufacturing (AM) of polymers has enabled 3D printed geometries suitable for custom parts. AM has potential uses in prosthetics, medical devices, wearable devices, optical components, and, more recently, shape morphing parts, known as 4D printing.[2–11] Current AM research strives to increase the printing speed, size, and material quality, while maintaining a low cost competitive with molding.[12,13] Recent 3D printing developments focus on increasing the printing speed by increasing the curing power delivery and compensating this added power with active cooling, which unfortunately increase the energy requirement and the process complexity.[14]

The growth of natural creatures follows a completely different manufacturing paradigm from AM. While in AM each voxel is digitally defined and deterministically deposited or photo-cured, organisms grow according to a genomic developmental plan describing the rates of cell division. Cell division on its own creates isotropic radial growth. However, natural organisms do have complex morphologies because cell division is modulated by physical cues, such as mechanical forces and chemical gradients which follow the developmental plan.[15] Natural growth is sustainable, realizes complex shapes, and does not need molds or sophisticated equipment. Natural growth requires a developmental plan which describes the growth process via information encoded in the genes, instead of a voxel-based description using computer-aided design (CAD).

2. Results and Discussions

2.1. Growth Printing Enabled by Frontal Polymerization

Here, we describe growth printing (GP): a 3D printing paradigm inspired by morphogenesis. GP is similar to tree growth,

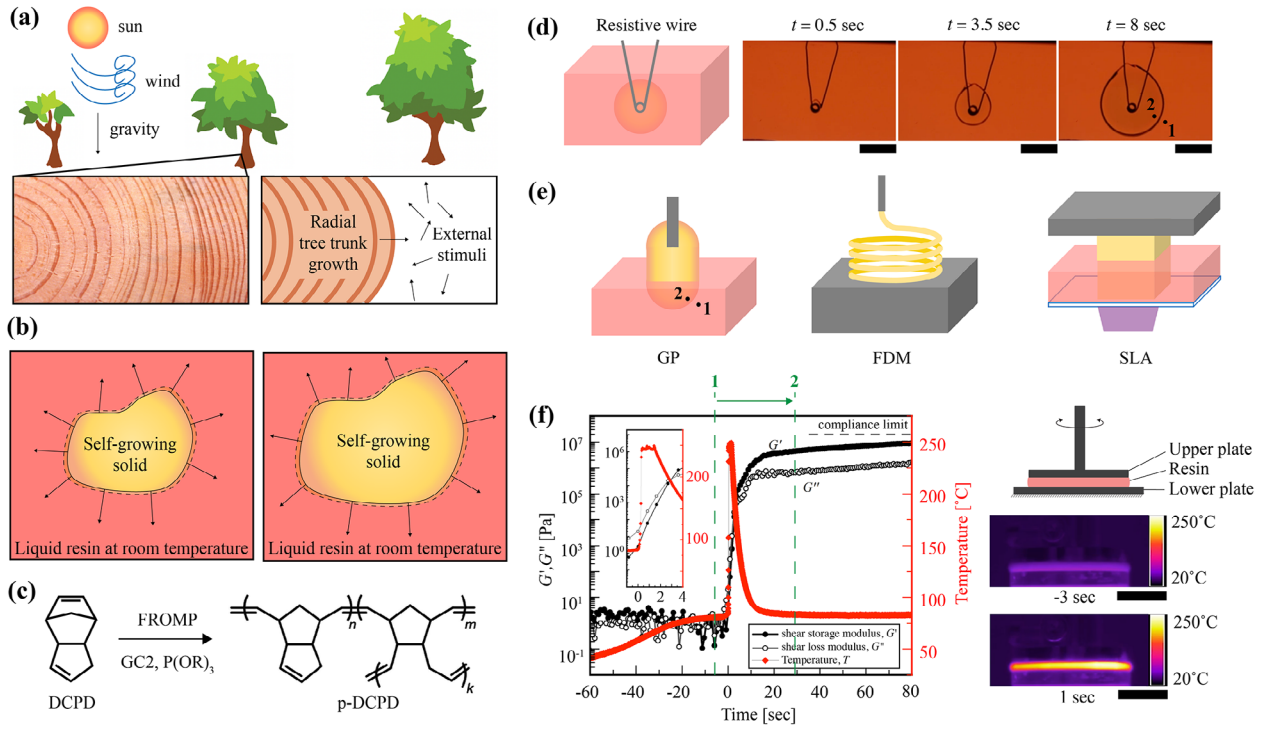

Figure 1. Morphogenic growth printing (GP). a) Morphogenesis of a tree trunk in its natural environment; b) Schematic of a radially-propagating polymerizing front which produces a self-growing solid object by consuming the surrounding monomers. The solid and dashed contour lines indicate the polymerized solid and the advancemet of the reactive front, respectively; c) Chemical reaction describing the frontal ring-opening metathesis polymerization (FROMP) of dicyclopentadiene (DCPD) into pDCPD. GC2 is Grubbs' second-generation catalyst and $P(OR)_3$ is a phosphite-based inhibitor used to control FROMP reactivity; d) Experiment of thermally-triggered FROMP nucleation and growth of a solid sphere using v-shaped resistive wire coiled at its tip; e) Schematics of GP, fused deposition modeling (FDM), and stereolithography (SLA). Labels 1 and 2 point to the liquid resin and the polymerized solid, respectively; f) Storage modulus G', loss modulus G'' and temperatures were obtained via a combination of rotational shear rheometry and IR video. Schematic and IR snapshots taken during in situ FROMP on the rheometer. All scale bars are 10 mm.

whereby new circumferential layers of cells are intrinsically added onto the trunk periphery (**Figure 1a**). As will be described later, GP also emulates how external stimuli, including gravity, wind, temperature fluctuations, and direction of exposure to sun, modulate the tree morphology.

In GP, the curing is self-energized by the exothermic frontal ring-opening metathesis polymerization (FROMP) reaction, which, once initiated, self-propagates spatially from a nucleus to instantly cure and solidify dicyclopentadiene (DCPD) liquid monomers.[16–18] DCPD forms poly-DCPD (pDCPD), a thermosetting polymer network via Grubbs' second generation catalyst (GC2) (Figure 1b). Tributyl phosphite ($P(OR)_3$) is an inhibitor that regulates and controls the rate of reaction before and after initiation. In ambient conditions, the cured pDCPD solid would continue to grow from a small initiation nucleus without any external supplied energy until all monomer is consumed. The FROMP reaction is triggered by a localized heat source to elevate the temperature of the nucleus to about 70 °C. The growth front self-propagates with a linear speed normal to the liquid–solid interface and hence arbitrary shapes of large sizes can be formed (Figure 1c). In Figure 1d, a resistive wire coiled into a spool of 3 mm diameter (with 5 turns within the spool) is powered with 5 W power input to trigger the FROMP reaction. Within a second, a pDCPD sphere forms and continues to grow with a radial front speed u_f^0 of 1.12 mm s^{-1} given an initial resin temperature T_0 = 20 °C. Parallel to this isotropic growth, GP uses a motion stage to pull the growing solid through the resin-air interface that defines the geometry of the produced part (Figure 1e). GP is hence a morphogenic manufacturing – different from traditional layer-by-layer voxel addition used in fused deposition modeling (FDM) or stereolithography (SLA) – because the growth continues like an organoid culture and the geometry is formed by external gradients of monomer.

GP is enabled because a liquid monomer with viscosity around 4.9 mPa.s (Point 1) is rapidly converted to polymerized solid with a storage modulus of > 10 MPa (Point 2) across a narrow (~1 mm) polymerization front. To capture this rapid phase transition, we conducted a curing reaction during oscillatory shear rheometry, carefully considering machine compliance limits.[19] FROMP of DPCD was conducted on a parallel plate rheometer (DHR-3, TA Instruments) using disposable, 25 mm diameter plates with 1.7 mm gap. A Peltier element heater was set to 90 °C to initiate the FROMP reaction between the plates and an oscillation stress amplitude of 100 Pa was applied at 10 Hz to measure the storage and loss moduli. As shown in Figure 1f, a rapid increase in shear storage modulus is observed at the onset of the FROMP reaction. We observe a four orders of magnitude increase in modulus in 4 s in parallel with an increase in temperature up to 250 °C within a

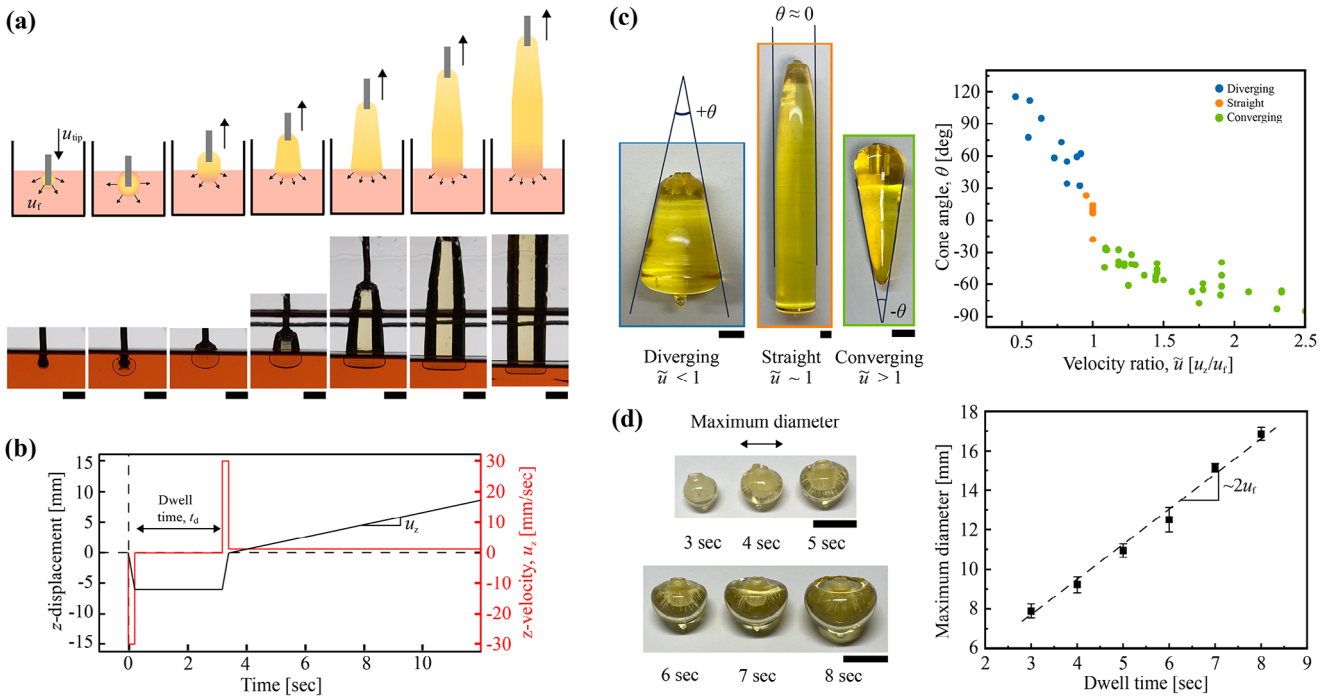

Figure 2. GP concept and demonstrations. a) Schematics (top) and photographs (bottom) of GP of a cylindrical (straight) shape; b) Tip motion profile used to produce the straight shape in a); c) Geometric control of diverging, straight, and converging shapes by increasing the tip velocity to front velocity ratio $\tilde{u}$; d) Radial control of semi-spherical prints by increasing the dwell times from 3 to 8 s. All scale bars are 10 mm.

few seconds due to the highly exothermic FROMP reaction. The solid material soon cools to around 90 °C due to diffusion of heat to the plates. After solidification, pDCPD has a storage modulus of around $2 \cdot 10^8$ Pa. A video of this experiment is provided in the Supporting Information (SV2) and related descriptions of the rheological measurements can be found in Supporting Information.

2.2. Growth Printing of Axisymmetric Parts

In the simplest GP process to produce axisymmetric shapes, the tip is mounted on a motion stage, heated to ~100 °C, and positioned 1 mm above the air-resin interface. The resin is in a glass container submerged in a larger ice water bath to control the temperature during the exothermic reaction. **Figure 2a** shows schematic and optical images of the GP manufacturing of a long cylindrical (straight) shape. A simple tip motion profile consists of the following 4 steps (Figure 2b): (1) dipping (downward motion), (2) dwell, (3) "un-dipping" (fast upward motion), and (4) upward motion at a prescribed velocity. The dipping step typically involves a 5 mm downward motion ($-z$ direction) at 30 mm s^{-1} and the "un-dipping step" is a 5 mm upward motion with the same speed. The dwell time t_d is the holding step between steps 1 and 3. As shown in the experimental results presented in Figure 2c, the part geometry depends on the ratio of the tip velocity and the front velocity $\tilde{u} = u_z/u_f^0$. If the tip moves slower than the front ($\tilde{u} < 1$), the front continuously grows to a larger lateral size, forming a diverging shape. If the tip moves faster than the front ($\tilde{u} > 1$), the growing part converges to a point. If the two are nearly the same ($\tilde{u} \approx 1$), the front maintains its lateral extent, producing a straight shape. The shapes of the printed parts are categorized by the cone angle θ. Positive cone angle $+\theta$ in the left image of Figure 2c indicates diverging shape, nearly zero as straight, and negative as converging shape. The dependence of θ on $\tilde{u}$ is presented in the Figure 2c. The effect of the dwell time on the size of the print is shown in Figure 2d. During the dwell time, the tip holds its position and allows the polymerization front to propagate freely in the resin bath, forming an initial spherical shape.

2.3. Numerical Modeling of Growth Printing: Forward and Inverse Problems

To simulate the GP process, we numerically solve the following coupled reaction-diffusion equations:

$$\rho c_p \frac{\partial T}{\partial t} = \kappa \mathcal{H}_{\mathrm{AD}} \nabla^2 T + \rho H_r \frac{\partial \alpha}{\partial t} - h\left(T - T_{\mathrm{amb}}\right)\left|\nabla \mathcal{H}_{\mathrm{AD}}\right|,$$
$$\frac{\partial \alpha}{\partial t} = A \exp\left(-\frac{E}{RT}\right)(1-\alpha)^n \mathcal{H}_{\mathrm{int}} \quad (1)$$

where the temperature T and degree of cure α are the variables of interest. The first relation in Equation (1) models the heat diffusion with ρ, c_p, and κ respectively denoting the density, specific heat, and thermal conductivity of the resin, and H_r is the heat generated by the exothermic reaction. The last term in that relation approximates the heat loss at the DCPD-air interface, with h denoting the heat transfer 'film' coefficient and T_{amb} the ambient

temperature. The second relation describes the cure kinetics of DCPD modeled in the form of an Arrhenius relation, with A, E, and R respectively denoting the rate constant, activation energy, and ideal gas constant.

The parameters A, E, and n from[20] reproduce front velocity and temperature consistent with experiments.

A schematic of the axisymmetric simulation problem is shown in **Figure 3**a. We adopt an axis system attached to the heated tip while the immersed free surface progressively raised or lowered to capture the relative motion of the tip. A description of the initial and boundary conditions and additional details on the simulations can be found in Supporting Information. The additional terms in Equation (1) correspond to the smeared Heaviside functions $\mathcal{H}_{\text{int}}$, $\mathcal{H}_{\alpha}$, and $\mathcal{H}_{\text{AD}}$ used for tracking the air–liquid resin free surface, the reaction front, and the air-pDCPD interface, respectively, and defined by

$$\mathcal{H}_{\text{int}} = \mathcal{H}\left(z_{\text{int}}(t) - z\right), \mathcal{H}_{\alpha} = \left(\alpha - \alpha_0\right)/\left(1 - \alpha_0\right), \\ \mathcal{H}_{\text{AD}} = \max\left(\mathcal{H}_{\alpha}, \mathcal{H}_{\text{int}}\right) \tag{2}$$

In Equation (2), $z_{\text{int}}(t)$ is the vertical location of the free resin surface, $\mathcal{H}(\phi) = 1/(1 + \exp(2.5\phi/\Delta x))$ is a smeared Heaviside function with Δx denoting the minimum grid size, and α_0 is the initial degree of cure. As was the case in previous FROMP-related studies,[21,22] the coupled reaction-diffusion equations are implemented in the finite-element-based Multiphysics Object-Oriented Simulation Environment (MOOSE),[23] taking advantage of its robust mesh adaptivity capability needed to capture the sharp, moving polymerization front.

In the present study, the reaction-diffusion model is used in two ways: (i) to solve the "forward problem" and predict the shape of the manufactured part for a given motion of the heated tip, and (ii) to solve the 'inverse problem' and predict the motion of the heated tip needed to achieve a target shape of the printed part.

In Figure 3b, the experimentally measured and computed shapes of the printed parts are compared for various values of the velocity ratio $\tilde{u}$. The computational models successfully capture the main features of the printed parts with divergent, straight, convergent, and corrugated profiles. These corrugated parts are obtained by adopting an intermittent upward motion of the tip, as shown in the Supporting Information video (SV3). Figure 3c presents a direct comparison between the observed and computed evolution of the shape of the printed part during the FROMP-based GP.

We adapt this model to calculate the required motion profile to produce a certain shape – which we refer to as the inverse problem. In the solution of the "inverse problem," the axisymmetric target shapes are expressed by nonuniform rational B-spline (NURBS) curves.[24] We expect the reaction front to gradually fill the area enclosed by the target shape but not beyond it by properly tuning z_{int}; therefore, at each time step $t = t_i$, the location of the free surface z_{int} is updated to the intersection point (r_i, z_{int}) between the reaction front (the $\alpha = 0.5$) and the target shape. After the simulation, t_i, r_i, and z_{int} are transformed to z_{tip} and the corresponding G-code. Three examples of inverse problems taken from natural products (raspberry, squash, and pine cone) are presented in Figure 3d–f. For each case, we provide the initial photograph, the NURBS curve, the predicted motion (displacement and speed) of the heated tip, the printed part based on the G-code, and a comparison between printed and target shapes. In the predicted tip motion plots, the dashed horizontal red line refers to the steady-state planar front propagation velocity ($\tilde{u} = 1$). The printed shapes in Figure 3d–f are controlled by the velocity ratio $\tilde{u}$. In the raspberry case, the tip begins with $\tilde{u} < 1$ to form the diverging upper region and transitions sharply to $\tilde{u} > 1$ at the converging region near the bottom (Figure 3d). In the squash case (Figure 3d), the velocity profile starts with $\tilde{u} \gg 1$ to capture the shape transition from a nearly spherical shape to the lower curvature. The tip velocity in the case of the pine cone (Figure 3f) is almost constant, although the steady tip velocity $\tilde{u}$ is slightly lower than 1 due to resin consumption and curvature-dependent heat diffusion. It is remarkable that the predictions of the inverse problem lead to a good match between the target and printed parts despite the relative simplicity of the modeling which ignores convection in the liquid, employs a heuristic chemical kinetic model, and relies on an approximate thermal boundary condition of the initiator.

2.4. Growth Printing of Asymmetric Parts

Beyond axisymmetric parts, four distinct approaches demonstrate the ability of GP to produce complex 3D parts: the cross section design of the tip, multiple tips with merging fronts, complex trajectories with angular motion of the tip, and resin viscosity modification (**Figure 4**). Figure 4a shows cases with asymmetry of the cross-section defined by the initiator shape. These shapes are different than the cylindrical initiator used in Figure 2 and 3. Here, the initiator breaks symmetry with a 3-fin tip (Figure 4a). When this geometry contacts the resin, the front initially follows the tip geometry, while the part is simultaneously pulled up out of the resin vat. As GP proceeds, sharp corners get more rounded, i.e., the curvature decreases, due to the radial nature of reaction-diffusion propagation. As a result, a part which is initially triangular near the initiator becomes more circular near its bottom. A different approach uses two cylindrical heaters instead of one heater, whereby the distance between the two heaters enables the two distinct fronts emerging from each heater to eventually merge during the production of the part (Figure 4b) where the spacing between the two tips is 15 mm. When two active fronts merge, they recover almost fully the mechanical strength of cured pDCPD at the interface (see Supporting Information). Third, symmetry can be broken lengthwise by complex tip trajectories which include angular motion to produce curved circular beams (Figure 4c). The cartridge heater is attached to a motor which rotates at constant angular velocity while the linear motions compensate for the initiator rotation such that the front remains localized at the DCPD air interface. The vertical motion is a function of the angular velocity and the natural speed of the front which is around 1 mm s^{-1}. The horizontal motion profile maintains the active front location in the resin vat, but this constraint can be relieved if an arbitrarily large resin container is used.

A final approach to break symmetry is to modify the rheological properties of the resin to sustain a stretched liquid bridge that contains and guides the solidification front (Figure 4d). A liquid bridge is formed when the solidification front is lifted above

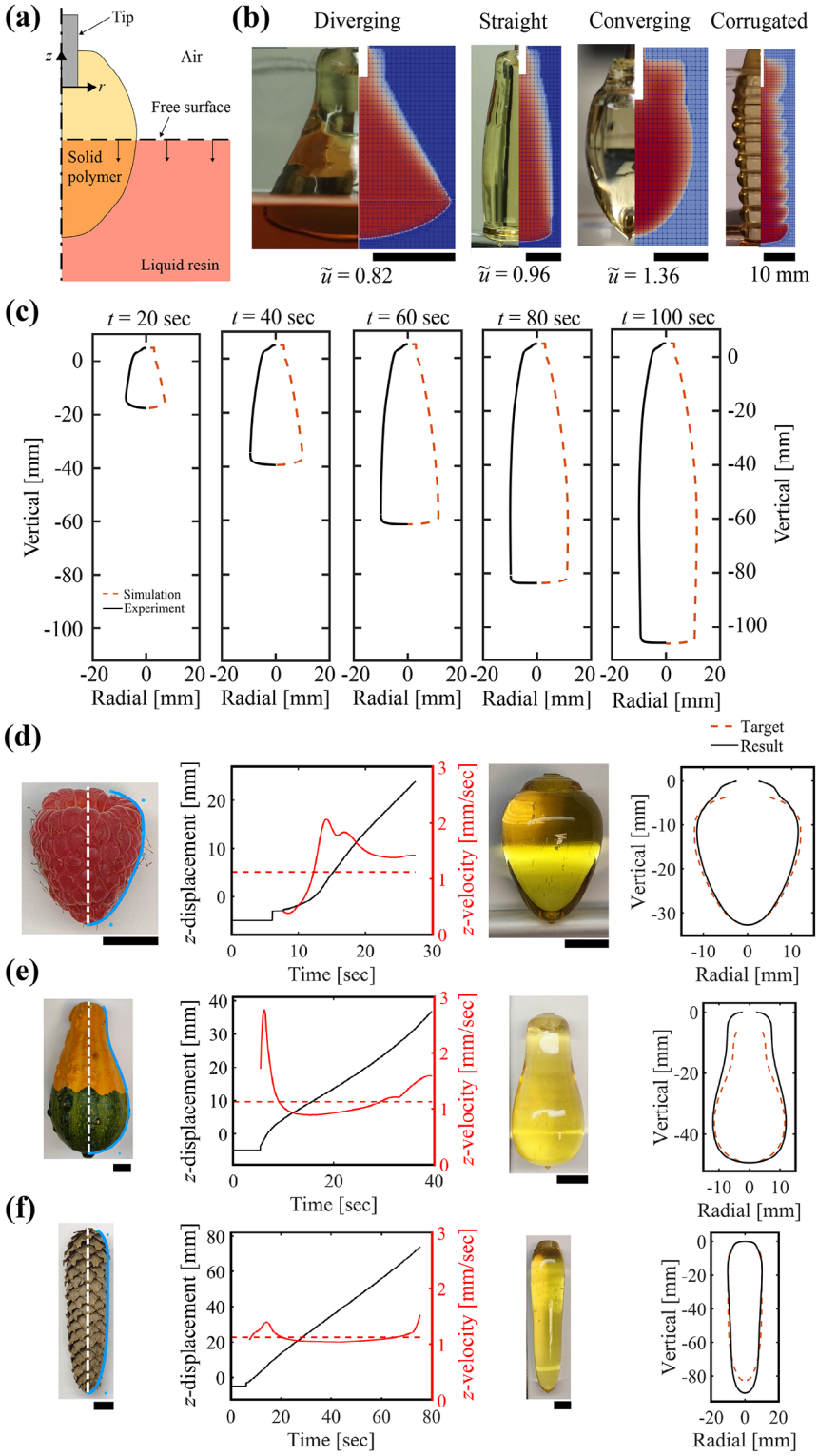

Figure 3. Simulation of GP with specified heated tip motion (forward problem) and growth printing for four axisymmetric shapes of natural produce using the G-codes generated by the numerical solver (inverse problem). a) Simulation schematic; b) Comparison between experimental and simulated shapes obtained for 3 values of $\tilde{u}$ leading to diverging, straight, and converging profiles. For the corrugated shape, the vertical motion of the heated tip consists of a succession of dwells and upward motions. c) GP of a straight shape: comparison between experiment (solid black) and simulation (dashed red) results at 5 different times. d) Growth printed raspberry. The control points and NURBS curve (blue) fitted as target shape. Inverse tip displacement (black), tip speed (red solid) and $\tilde{u} = 1$ reference (red dashed) versus time. Comparison between target and printed shapes; e) Squash; f) Pinecone; All scale bars are 10 mm.

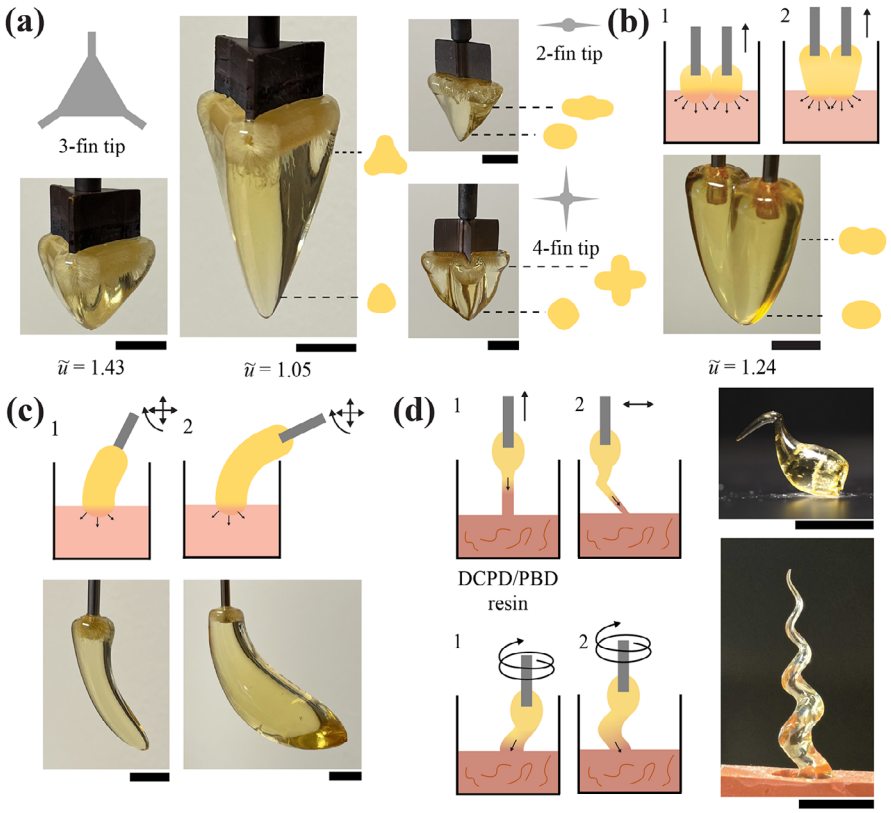

Figure 4. Symmetry breaking in GP. a) Tip shapes break axisymmetry. 2, 3, 4-fin tips and the resulting cross-section change during GP; b) Two parallel tips. A front initiates from each tip then they merge in the middle between them during the motion; c) Curved circular beams made through tip horizontal, vertical, and angular motion trajectories. The left and right parts were produced with different dwell time, 4.5 and 5.5 s; d) Viscosity-modified resin enabling a front within the pulled viscous filament. Here, the polymerizing front can propagate in the resin filament out of the vat. By imposition horizontal or helical tip motion, a kiwi bird and helical horn shapes are produced, respectively.

the far-field horizontal air–liquid resin free surface, e.g., to define the end of the part. Importantly, the DCPD resin used in all other cases in this study except Figure 4d has low viscosity; and hence any liquid bridge formed by lifting the tip breaks quickly. We hypothesized that with sufficiently high extensional viscosity and within a certain range of off-vertical velocity of the tip, an inclined liquid bridge could be created that contains the solidification front and guides its path to create more complex and asymmetric patterns. We increased resin viscosity while retaining successful FROMP reactivity by adding polybutadiene (PBD, average molecular weight 200 000–300 000) at 15 wt% into the DCPD monomer resin. We are not aware of this formulation being reported before, but PBD and pDCPD have been reported as co-polymer constituents resulting from FROMP reaction of a mixture of their co-monomers.[25] The zero-shear viscosity of the resin was increased from $\eta_0 = 4.9 \cdot 10^{-3}$ Pa·s to $\eta_0 = 28.5$ Pa·s (see Supporting Information for detailed rheological and mechanical characterization). This rheology-modified resin successfully sustains a liquid bridge using zig-zag and helical trajectories, localizing the front within the bridge to freeze these complex shapes (Figure 4d). For example, a kiwi bird shape is produced by first producing the body during the isotropic radial growth of the front during the dwell time, followed by a zigzag upward trajectory to form the neck, head, and beak. Similarly, a helical horn shape is produced by helical motion of the initiator. Details of the printing conditions and the fabrication processes can be found in the Supporting Information and SV5. Several rheological properties may be responsible[26] for successfully achieving this processing flow. In this case, for these flow conditions, we attribute the increased extensional viscosity to be associated with the low strain rate (low Weissenberg number) regime, and therefore associated primarily with the increase in η_0, rather than exploiting viscoelastic stresses or extensional thickening due to stretching of the PBD polymer chains (see Supporting Information).

2.5. Benchmarking Growth Printing Speed and Energy Use

The GP process presents two major advantages: high print speed and low manufacturing energy as shown in **Figure 5**. On this chart, we compare the FROMP-based GP and direct ink writing to other commercially available additive manufacturing processes in terms of volumetric print rate $\dot{V}$ [mm^3/hr] and specific energy consumption (SEC) [MJ/kg]. Processes that are fast, with low total energy input, are in the upper left. Existing manufacturing processes require continuous energy input to the printer from start to end, for example to melt the material (FDM) or for photo crosslinking (SLA). In contrast, GP only requires a very small amount of energy (typically ~ 10 J) to initially trigger the exothermic FROMP reaction. Therefore, larger print volumes have a

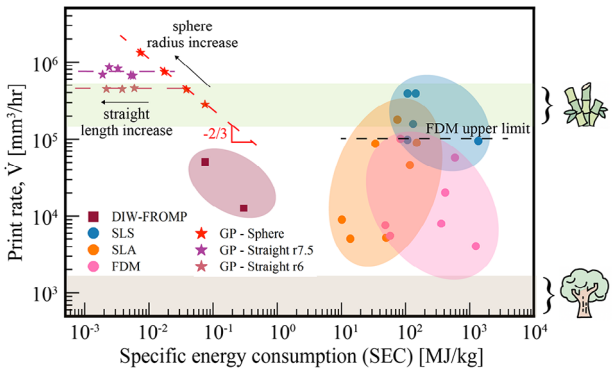

Figure 5. Print rate and specific energy consumption (SEC) of various additive manufacturing processes. The trends associated with GP process measurements (star symbols and dashed lines) are discussed in the text. GP data points (star) are measured from GP experiments. r is the radius in mm of printing spheres or straight cylinders.

continually decreasing SEC, since the external energy input is finite but the volume continues to grow, as shown by GP data progressively populating to the left with larger sizes. The printing rate of GP is governed by the front propagation speed, which is approximately 1 mm s^{-1} for DCPD at room temperature. When growth occurs along only one direction, as with a straight cylindrical part, the volumetric print rate is a constant proportional to the front speed, yielding a horizontal trend line in Figure 5. However, when printing occurs in multiple directions, the volumetric growth rate increases with the size of the part. For example, with a spherical shape, the volumetric growth rate is proportional to the product of the sphere surface area and front speed. Hence, larger parts can have higher volumetric print rates, shown with the sphere data trending higher with increasing radius. The resulting power law of $\dot{V} \sim \mathrm{SEC}^{-2/3}$ for the sphere is associated with volume-dependence for SEC and the surface area dependence for $\dot{V}$ with a constant propagation speed (red star symbols and dashed red curve in Figure 5). FROMP-based direct ink write (DIW)[27,28] has the same advantage of low curing energy consumption, but its print rate is limited by its nozzle diameter, not by the part size, and is therefore much lower than GP's print rate. An analysis of the other AM processes can be found in the Supporting Information.

3. Conclusion

In summary, we have demonstrated a new morphogenic 3D growth printing process for fast and energy-efficient manufacturing of polymer parts. GP relies on the self-propagating polymerization reaction initiated in a resin vat combined with tip motion. This unique process has various advantages including low energy consumption (at least 3 orders of magnitude lower energy consumption than SLA) and fast speed (2 to 10× faster than the fastest SLA). We describe this manufacturing as morphogenic, a word which describes how geometries are defined in natural organisms during growth. The term *genesis* captures the idea that living cells divide and self-replicate. This replication forms isotropically growing spherical organoids in the absence of external forces or chemical gradients. The term *morpho* captures the idea that the shape of growing organoids - which is usually intrinsically isotropic- morphs by external mechanical forces and chemical gradients. GP is hence a morphogenic manufacturing because the growth continues naturally by the self-propagating chemical reaction like the *genesis* of an organoid and the geometry *morphs* by external gradient of the monomer. We developed numerical solutions of the reaction-diffusion equation and a geometric algorithm that resolves and tracks the interface between the solid, liquid, and air phases to enable the inverse design of various bio-inspired shapes. More complex geometries are demonstrated using several approaches including multi degree of freedom initiator motion, initiator tip shape design, and rheologically modifying the resin. Future work includes expanding on these geometric capabilities and expanding the current numerical models to capture the asymmetric geometries and the interesting hydrodynamic effects (e.g., convective and Marangoni flows) which would be encountered in that process.[20,29]

4. Experimental Section

Resin Preparation: Dicyclopentadiene (99 pure DCPD, Ultrene) is solid at room temperature. Solid DCPD is heated to 50°C to the liquid state and mixed with 5-Ethylidene-2-norbornene (ENB, Sigma-Aldrich) in 95:5 wt% ratio. This mixture is liquid at room temperature. The mixed monomers are filtered through aluminum oxide powders (Sigma-Aldrich) to remove inhibitors present in the raw materials received from the manufacturer. In a typical growth-printing experiment, 60 mg of Grubb's catalyst M204 (GC2, Sigma-Aldrich) are mixed to 3 mL phenylcyclohexane (PCH, Sigma-Aldrich) and sonicated about 3 min. 19.1 µL tributhyl phosphite (TBP, Sigma-Aldrich) are then added to the catalyst solution in a nitrogen glove box, and the prepared catalyst solution is added to 93.2 g DCPD/ENB. The final resin composition is GC2:DCPD/ENB:TBP:PCH = 1 mg: 1.553 g: 0.319 µL: 50 µL, which is identical to what used in the work of Robertson et al. (DCPD:GC2:TBP 10000:1:1).[16]

Growth Printing Setup: Approximately 100 g of resin are poured into a 65 × 65 × 65 mm^3 cubic glass beaker. The straight side walls of the beaker enable side-view optical photography. The resin bath is inserted into a larger 110 × 110 × 110 mm^3 beaker filled with water (15 ± 2 °C) to regulate the temperature of the resin bath 20 ± 1 °C during the experiments. A cartridge heater of 1/8 inch diameter and 2 inch length (MCH2-80W-001, Comstat) is mounted to the motion stage (A3200, Aerotech). With 5 W of power supplied to The cartridge heater, the tip reaches approximately 100 °C before being dipped into the resin bath. The motion profile is programmed in G-code and executed to conduct the vertical motion for growth printing. A DSLR Camera (EOS R5, Canon) is used to capture side-view videos.

Asymmetric Growth Printing Setup: 2,3, and 4-fin tips: The copper tips are waterjet cut to the shape from copper plate (145 copper, McMaster-Carr) and mounted to the soldering iron. The tip is heated to 200 °C, to ensure instant initiation of FROMP reaction but not to induce excessive bubble generation and burning the cured resin. Dwell time ranges 5–7 s and tip z-velocities are 1.1–1.3 mm s^{-1}. To take bottom view images, a cube support structure is fabricated using 20/80 aluminum T-frames. The resin vat and cooling bath sit on an transparent acrylic plate at the top of the bottom structure. A mirror at 45 degree angle is inserted in the bottom structure to capture bottom view image using a camera.

Double tips: Two identical cartridge heater tips are mounted to machined ceramic block (Macor, Corning) with two holes machined to fit heaters in spacing of 15 mm. Then the block is mounted to the linear stage and GPed with dwell of 5 s and linear z-velocity of 0.9–1.3 mm s^{-1}.

Rotational tip: The cartridge heater is mounted on a motor (NEMA 17 motor with 51:1 planetary gear ratio, Stpperonline) using 3D-printed guide (Form 3 using high-temp resin V2, Formlabs). The motor is controlled using an arduino board (Arduino Mega 2560) and synchronized the rotational motion to the linear stage. The linear stage motion is modified

using custom G code to fix the active front in the resin vat, accounting for the rotational motion (0.0245 rad s^{-1}) of the tip. The target z-velocity ratio is 1 to produce long straight print, which is used for straight print in the main text.

Viscosity modified resin: 15t% of polybutadiene (PBD-cis, Sigma-Aldrich) of average molecular weight of 200–300k is mixed to the DCPD and stirred for one full day using a stir bar. The same amount of GC2 catalyst solution is added to prepare the resin. The resin vat is then degassed for 2–3 min to remove most of the bubbles formed during the catalyst mixing. Rheology of the resin can be found in the Supporting Information Section S3.4. The tip is controlled with dwell time of 2 s and dipping and un-dipping speed is 10 mm s^{-1}. For kiwi-bird shapes, horizonal motion or slight inclination of 2–3 mm at 6 mm s^{-1} is imposed. Helix motion is radius of 6 mm, vertical 9 mm, at 3 mm s^{-1} speed.

Supporting Information

Supporting Information is available from the Wiley Online Library or from the author.

Acknowledgements

This work was supported by Regenerative Energy-Efficient Manufacturing of Thermoset Polymeric Materials (REMAT), an Energy Frontier Research Center funded by the U.S. Department of Energy, Office of Science, Basic Energy Sciences under Award DE-SC0023457. [Correction added on May 5, 2025, after first online publication: author affiliation for Yuan Gao is corrected.]

Conflict of Interest

The authors declare no conflict of interest.

Author Contributions

M.Z. and M.T.H. contributed equally to this work. Y.S.K., M.Z., and M.T.H.: drafting the article, data analysis and interpretation, figure generation. Y.S.K.: growth printing experiment. M.Z., Y.G.: simulation. M.T.H.: designing, formulating, and using the viscosity-modified resin, conducting all rheology measurements. D.S., R.S.: experiments on asymmetric printing. J.S.M., N.S., R.H.E., P.H.G., S.H.T.: conception of the work, data analysis and interpretation, funding, revising the manuscript.

Data Availability Statement

The data that support the findings of this study are available from the corresponding author upon reasonable request.

Keywords

3D printing, additive manufacturing, bio-inspired manufacturing, frontal polymerization, reaction-diffusion

Received: May 1, 2024
Revised: January 29, 2025
Published online: March 10, 2025

[1] A. J. Timmis, A. Hodzic, L. Koh, M. Bonner, C. Soutis, A. W. Schäfer, L. Dray, *The International Journal of Life Cycle Assessment* **2015**, *20*, 233.
[2] R. K. Chen, Y. an Jin, J. Wensman, A. Shih, *Addit. Manuf.* **2016**, *12*, 77.
[3] L. Rosalia, C. Ozturk, D. Goswami, J. Bonnemain, S. X. Wang, B. Bonner, J. C. Weaver, R. Puri, S. Kapadia, C. T. Nguyen, E. T. Roche, *Sci. Rob.* **2023**, *8*, eade2184.
[4] A. Kalkal, S. Kumar, P. Kumar, R. Pradhan, M. Willander, G. Packirisamy, S. Kumar, B. D. Malhotra, *Addit. Manuf.* **2021**, *46*, 102088.
[5] K. Willis, E. Brockmeyer, S. Hudson, I. Poupyrev, in *Proceedings of the 25th Annual ACM Symposium on User Interface Software and Technology*, UIST '12, Association for Computing Machinery, New York, NY, USA, ISBN 9781450315807, **2012**, pp. 589–598.
[6] Z. Ding, C. Yuan, X. Peng, T. Wang, H. J. Qi, M. L. Dunn, *Sci. Adv.* **2017**, *3*, 1602890.
[7] A. Sydney Gladman, E. A. Matsumoto, R. G. Nuzzo, L. Mahadevan, J. A. Lewis, *Nat. Mater.* **2016**, *15*, 413.
[8] M. A. S. R. Saadi, A. Maguire, N. T. Pottackal, M. S. H. Thakur, M. M. Ikram, A. J. Hart, P. M. Ajayan, M. M. Rahman, *Adv. Mater.* **2022**, *34*, 2108855.
[9] R. L. Truby, J. A. Lewis, *Nature* **2016**, *540*, 371.
[10] M. Hua, D. Wu, S. Wu, Y. Ma, Y. Alsaid, X. He, *ACS Appl. Mater. Interfaces* **2021**, *13*, 12689.
[11] Y. Wang, R. Yin, L. Jin, M. Liu, Y. Gao, J. Raney, S. Yang, *Adv. Funct. Mater.* **2023**, *33*, 2210614.
[12] K. Yang, J. C. Grant, P. Lamey, A. Joshi-Imre, B. R. Lund, R. A. Smaldone, W. Voit, *Adv. Funct. Mater.* **2017**, *27*, 1700318.
[13] J. Go, S. N. Schiffres, A. G. Stevens, A. J. Hart, *Addit. Manuf.* **2017**, *16*, 1.
[14] D. A. Walker, J. L. Hedrick, C. A. Mirkin, *Science* **2019**, *366*, 360.
[15] T. Lecuit, L. Mahadevan, *Development* **2017**, *144*, 4197.
[16] I. Robertson, M. Yourdkhani, P. Centellas, J. En Aw, D. G. Ivanoff, E. Goli, E. M. Lloyd, L. M. Dean, N. R. Sottos, P. H. Geubelle, J. S. Moore, S. R. White, *Nature* **2018**, *557*, 223.
[17] B. A. Suslick, J. Hemmer, B. R. Groce, K. J. Stawiasz, P. H. Geubelle, G. Malucelli, A. Mariani, J. S. Moore, J. A. Pojman, N. R. Sottos, *Chem. Rev.* **2023**, *123*, 3237.
[18] J. A. Pojman, *Polymer Science: A Comprehensive Reference Vol. 4*, Elsevier, **2012**.
[19] M. T. Hossain, C. W. Macosko, G. H. McKinley, R. H. Ewoldt, *Rheol. Acta* **2025**, *64*, 67.
[20] Y. Gao, J. E. Paul, M. Chen, L. Hong, L. P. Chamorro, N. R. Sottos, P. H. Geubelle, *Phys. Rev. Lett.* **2023**, *130*, 028101.
[21] E. Goli, T. Gai, P. H. Geubelle, *J. Phys. Chem. B* **2020**, *124*, 6404.
[22] S. Vyas, X. Zhang, E. Goli, P. Geubelle, *Compos. Sci. Technol.* **2020**, *198*, 108303.
[23] A. D. Lindsay, D. R. Gaston, C. J. Permann, J. M. Miller, D. Andrš, A. E. Slaughter, F. Kong, J. Hansel, R. W. Carlsen, C. Icenhour, L. Harbour, G. L. Giudicelli, R. H. Stogner, P. German, J. Badger, S. Biswas, L. Chapuis, C. Green, J. Hales, T. Hu, W. Jiang, Y. S. Jung, C. Matthews, Y. Miao, A. Novak, J. W. Peterson, Z. M. Prince, A. Rovinelli, S. Schunert, D. Schwen, et al., *SoftwareX* **2022**, *20*, 101202.
[24] L. Piegl, W. Tiller, *The NURBS Book*, Springer-Verlag, Berlin, Heidelberg **1995**.
[25] L. M. Dean, Q. Wu, O. Alshangiti, J. S. Moore, N. R. Sottos, *ACS Macro Lett.* **2020**, *9*, 819.
[26] R. H. Ewoldt, C. Saengow, *Annu. Rev. Fluid Mech.* **2022**, *54*, 413.
[27] J. E. Aw, X. Zhang, A. Z. Nelson, L. M. Dean, M. Yourdkhani, R. H. Ewoldt, P. H. Geubelle, N. R. Sottos, *Adv. Mater. Technol.* **2022**, *7*, 2200230.
[28] M. Zakoworotny, F. J. Balta Bonner, A. Kumar, J. E. Aw, S. H. Tawfick, R. H. Ewoldt, N. R. Sottos, P. H. Geubelle, *Comp. Meth. Appl. Mech. Eng.* **2024**, *418*, 116565.
[29] A. Kumar, L. M. Dean, M. Yourdkhani, A. Guo, C. BenVau, N. R. Sottos, P. H. Geubelle, *J. Mech. Phys. Solids* **2022**, *168*, 105055.